Hydraulic characterization of a highly anthropized coastal aquifer subject to tidal fluctuations

Pierre Fischer, Abderrahim Jardani, M. Krimissa, C. Couegnas

Hydraulic characterization of a highly anthropized coastal aquifer subject to tidal fluctuations

P. Fischer[1], A. Jardani[1], M. Krimissa[2], C. Couegnas[2]

(1) Normandie Univ, UNIROUEN, UNICAEN, CNRS, M2C, GeoCNN Consortium, 76000 Rouen, France

(2) Electricité de France, EDF R&D, Laboratoire National d'Hydraulique et d'Environnement, 78401 Chatou, France

Conflict of interest: None

Corresponding author: P. Fischer

E-mail :

Key words:

Tide, Coastal aquifer, Hydraulic barrier, Inverse modeling, France

Abstract

The hydraulic characterization of a highly anthropized coastal aquifer in France is presented. The current industrial operations of the study site prevent the use of standard 'active' hydrogeological investigation methods (pumping, slug tests). However, the studied field is bordered on its north-western side by a channel directly connected to the sea, which allows for characterization of the hydraulic properties of the aquifer from its natural responses to the channel's tidal signal. Piezometers (37) were monitored, from which oscillatory water-level responses (amplitude and phase-offset) to the tidal signal were extracted through linear regression and fast Fourier transform. A two-dimensional (2D) numerical model in the frequency domain was built to simulate the oscillations. The anthropic buried walls and barriers existing at the site are represented as 1D elements in a 2D model representing the properties of the aquifer. A deterministic inversion process optimizes the spatial distribution of aquifer properties and anthropic-structure properties in the model, in order to minimize the differences between the responses simulated with the model and those measured in the field. The results of the characterization on this complex study case (flows highly constrained by hydraulic barriers or buildings, and the impossibility to perform pumping tests) generate simulations able to reproduce the observed responses. The property and simulation maps generated make it possible to take into account the impact of the anthropic structures on the groundwater flows and to localize the parts of the hydraulic barriers where most exchanges between the channel and the aquifer occur.

1. Introduction

Hydraulic tomography techniques aim to determine the spatial distribution of hydraulic properties (conductivity and storage) of an aquifer by analyzing the punctual piezometric fluctuations due to an hydraulic solicitation of the groundwater (Carrera and Neuman 1986 ; de Marsily et al. 1995 ; Yeh and Lee 2007). Commonly, in an hydraulic tomography investigation, the hydraulic data are generated through cross-hole injections or extractions of groundwater while measuring the hydraulic head in piezometers (Cardiff et al. 2009 ; Illman et al. 2009 ; Fischer et al. 2017). Generally, the interpretation of the hydraulic data is completed by an inversion algorithm in which the hydraulic diffusion equation is numerically solved until iteratively finding a model of hydraulic properties able to match the piezometric data. The accuracy of the retrieved model depends on the nature of the inversion algorithm (stochastic and deterministic), and the amount and the localization of the measurement points on the field. However, the applicability of this strategy is limited to the characterization of productive aquifers, and when the observation and pumping wells are close enough to record a significant hydraulic variation.

The practice of pumping tests on industrial sites is a complex and supervised operation that requires the agreement of the public authorities. For this reason, the ability to perform pumping tests in the industrial area studied in this work is very limited. Another particular difficulty of this area is the necessity to take into account the walls and barriers that constrain the groundwater flow in the soil. The characterization of these structures is essential as they modify the groundwater flow paths, but also because they are often built to limit risks of contamination. The localization of potential leakages in such natural or anthropic barriers has been studied with different types of solicitation signals by several researchers (among them Vilarrasa et al. 2011 ; Bolève et al. 2011 ; Sun et al. 2015). Alcolea et al. (2007) already took into account

heterogeneity due to anthropic structures in a zoned model of properties in order to constrain the preferential flow paths in the aquifer.

In the industrial study case reported here, the use of natural forces affecting the groundwater level, such as natural hydraulic level variations (D'Oria and Zanini 2019) or tidal variations induced by the lunar and solar forces (Rhoads and Robinson 1979), can be an interesting alternative when the use of active methods is limited. In particular, as this study site is situated along a channel directly connected to the sea, studying the groundwater responses to the natural tide appears to be the most appropriate option to derive the hydraulic properties of the aquifer and the barriers. In fact, the analysis of tidal oscillations provides a large-scale characterization of aquifers, including the hydraulic impact of some anthropogenic structures, such as the hydraulic barriers along the boundaries to the tidal source. This approach can be called 'passive', in comparison the 'active' approaches that require a human intervention to solicit water-table changes with oscillating signals (Bouwer and Rice 1976 ; Brauchler et al. 2010 ; Guiltinan and Becker 2015). In the hydroscience literature, many studies have been devoted to the identification of hydraulic properties by exploiting the tide component in piezometric fluctuations. Among them Rhoads and Robinson (1979) used different periodic water-level variations (through ocean, earth and barometric tide signals) measured in three wells during two months to estimate various aquifer parameters (including specific storage and porosity) from analytical solutions. However the accuracy of their estimates was limited by a possible leakage effect in the aquifer, considered as confined. More recently, Wang et al. (2018) extended the analytical solutions to the responses to earth tides in order to estimate the transmissivity, storativity and specific leakage in leaky aquifers. In the cases of a coastal or an island aquifer, the oceanic tidal forces become particularly interesting. Thus, Tefry and Bekele (2004) and Wen et al. (2018) used the responses of island aquifers to the oceanic tides to estimate their heterogeneous properties. Alcolea et al. (2007) associated sea tides and injection

wells to reconstruct the distributions of transmissivity and storativity in a coastal area. The properties of riverine aquifers can also be assessed through their responses to tidal signals when the river is large enough to permit a propagation of the oceanic tides, as shown for example in Jardani et al. (2012). In that study, the authors inverted the tidal responses of an alluvial aquifer to a river connected to a sea to estimate its distributions of transmissivity and vertical leakage. These oscillatory signals can be modeled in a frequency domain, instead of a time domain (Black and Kipp 1981; Black et al. 1987; Fischer et al. 2018a), which reduces the computation time of the inverse problem. This partly explains why oscillatory signals have become a topic of particular interest in hydraulic tomography (Cardiff et al. 2013 ; Zhou et al. 2016 ; Fischer et al. 2018b).

This study proposes a faster analysis of the hydraulic responses to the sea tidal fluctuation in the coastal aquifer by reformulating the transient mode of the inverse problem in a frequency domain. This work presents a new modeling method that permits one to simultaneously characterize the distributions of transmissivity and storativity in the aquifer and also localize potential leakages in hydraulic barriers by exploiting the natural sea tidal forces. This case study includes the anthropic structures and barriers in the inversion process in order to better simulate their impact on the complex flows on this site and to identify localizations, in these structures, where water exchanges between the aquifer and the channel are the most important. The paper first presents the study area, the dataset of measured hydraulic levels and the data processing that permits extraction of the tidal responses from the piezometric variations. Then the numerical model is presented, along with the inversion process that allows for a reconstruction of the properties in the model in order to reproduce the measured responses. Finally the results of the model are discussed in terms of reproduction of the responses and reconstruction of the distributions of transmissivity and storativity over the study area.

2. Site and data presentation

2.1. Study site

The study area is part of a highly anthropized industrial site located on the coast of France, half a kilometer away from the sea. The site is connected to the sea through a channel of 10 to 15 m depth. The study site involves an area of 1,300 × 500 m² along this channel, presented in Figure 1.

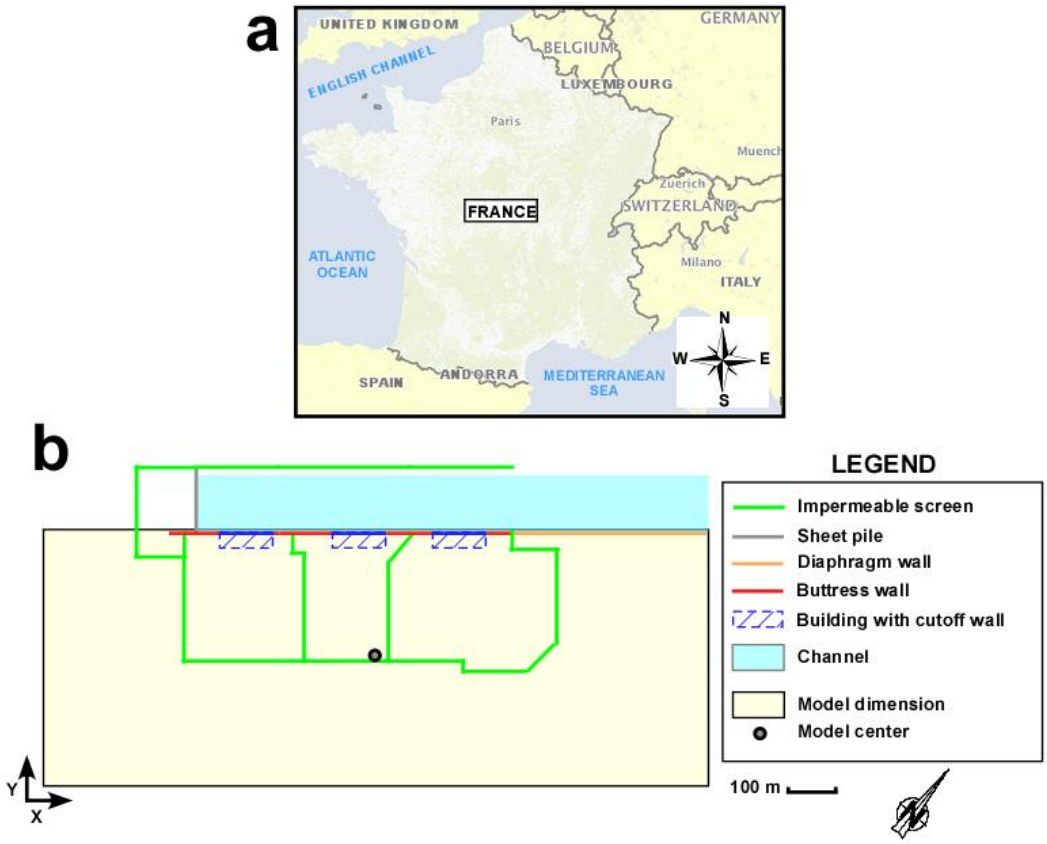

Figure 1: **a** Location of France. The study site is situated on the coast of France (the exact location of the site is not indicated due to the confidentiality requirements of the study). **b** Schematic top-down view of the site showing the location of the different anthropogenic structures, the channel and the area of interest for the hydraulic characterization.

This area is highly anthropized and its surface is almost totally concreted over (buildings or roads). Its subsurface is a 30-m thick heterogeneous aquifer, lying on impermeable clays, and composed of different layers of sands separated by discontinuous lenses of silts. The channel and existing anthropogenic structures in this field are installed in the upper part of this aquifer, in a sandy unit, partially connected to the bottom part of the aquifer. The groundwater in this aquifer is confined by the compaction of the surface soil on the study field, due to the anthropization of the whole site.

The groundwater flows in this area are constrained by buried 10–15 m deep sheet piles, barriers and walls (Figure 1) that have a thickness of 50 cm. The channel and the barriers are cutting through the confining surface soil and influence the groundwater flows. Three buildings, installed up to 16 m underground, located alongside the channel could also have an impact on the flows.

Therefore two strategies of two-dimensional (2D) modeling will be tested in this study, one that takes into account these buildings as constraints and the other not. It was decided to use 2D models instead of 3D ones because the dataset, composed of piezometric measures, is integrative and does not allow for a 3D characterization. Furthermore, 2D models are faster to solve and, therefore, allow for a higher resolution of property spatial distributions in the inversion processes. As, in this case, the groundwater flows in the investigated section (10 to 15 m depth) are mostly horizontal and perturbed by structures modifying locally this spatial distribution in the property fields, it is believed that modeling in a 2D top-down view is the best compromise of accuracy and time consumption.

2.2. Piezometric responses to the tidal signal

The piezometric responses in the aquifer are measured continuously and automatically each 15 minutes by probes in 37 piezometers distributed over the study area (Figure 2). These

piezometers were drilled to a depth of 10m and are screened from 5 m to 10 m depth. The hydraulic level in the channel is also measured automatically each hour by a probe. All these recorded data are saved in a private repository, property of Electricité de France (EDF).

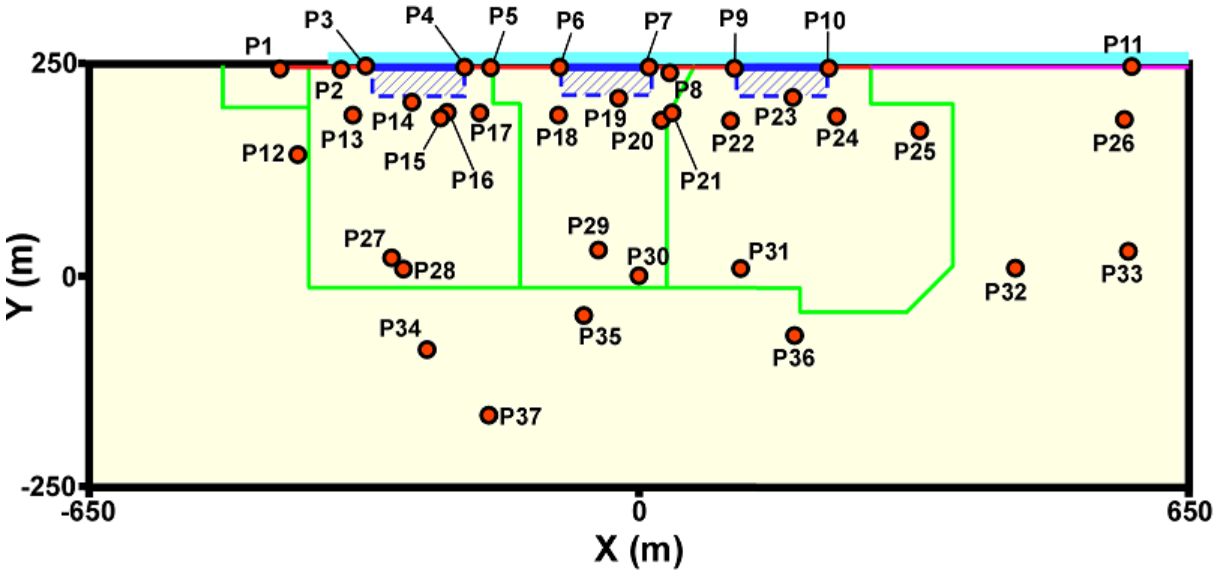

Figure 2: Location and designation of the 37 piezometers measuring continuously the groundwater level at the studied site.

As it is an industrial site in operation, it is too difficult to perform any pumping tests in the area. In this case, the use of the tidal oscillation as a solicitation signal is the most appropriate option to derive the hydraulic properties of the aquifer and the barriers. A piezometric dataset covering a period of four days of measurements in November 2016 was selected. During this period the rainfall recharge was particularly low (six consecutive days without rain), which meant that the groundwater responses to the tidal signal in the piezometric measurements could be more precise.

2.3. Data processing

It is noted that the piezometric level measurements in the field could be approximated as the sum of a linear response and an oscillatory response (see Figure 3):

$$h(x,y,t) \simeq h_{osc.}(x,y,t) + h_{lin.}(x,y,t) \quad (1)$$

with h the hydraulic level response over space and time in m, $h_{osc.}$ the oscillatory part of the response in m, and $h_{lin.}$ the linear part of the response in m, which represents an approximation of the non-tidal temporal trend in groundwater elevations.

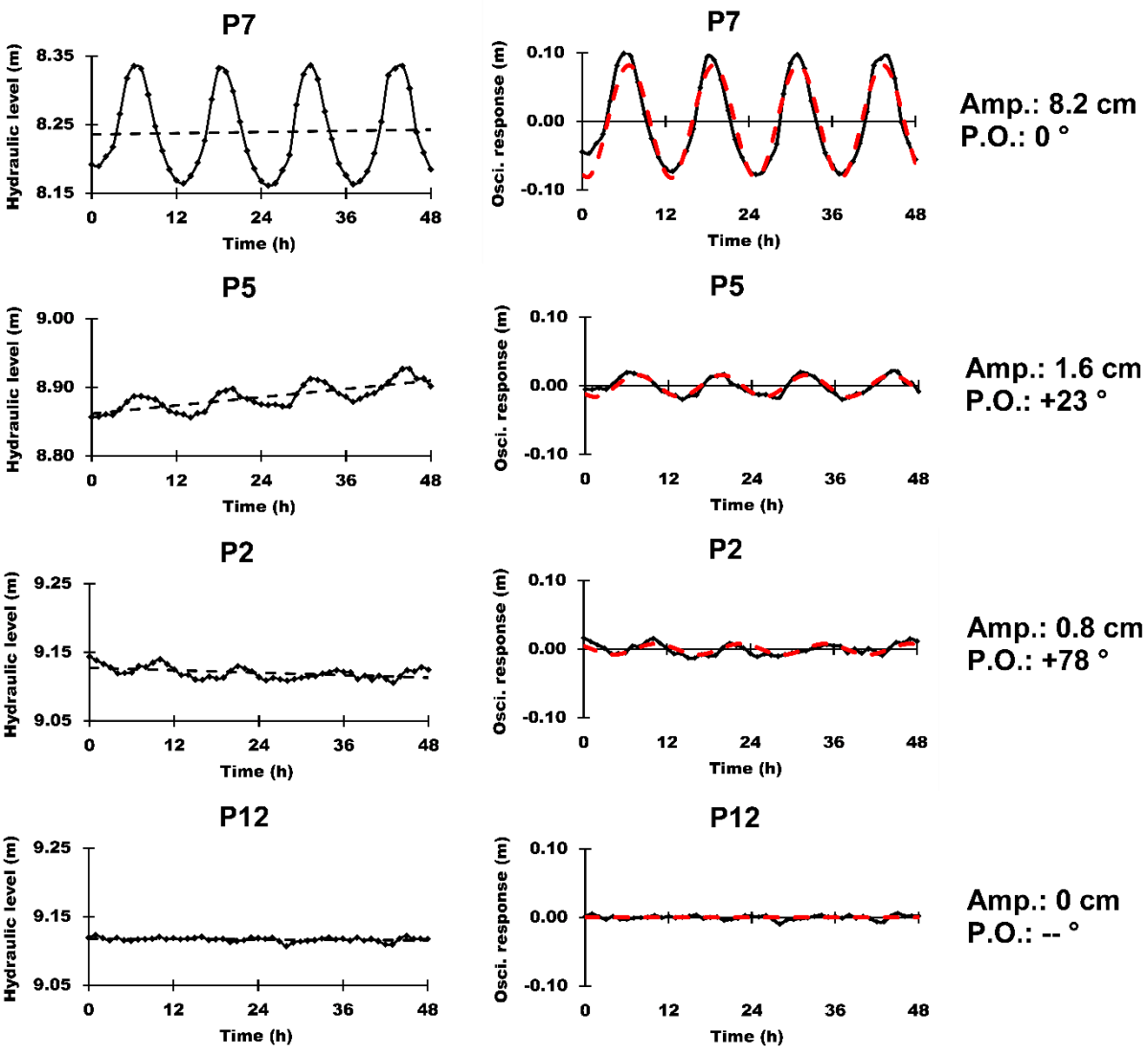

Figure 3: Example of data processing for four different piezometer (P7, P5, P2, P12) responses. In the left panel, a linear component (dotted lines), found through linear regression, is subtracted from the measured hydraulic level in order to assess only the oscillatory part of the response (Eq. 1). Then, in the right panel, a fast Fourier transform (FFT) is performed (red dashed lines) on the oscillatory part (black lines) to interpret the response of each piezometer in terms of amplitude (Amp.) and phase-offset (P.O.). The phase-offset responses are calculated relative to the signal of P7, the piezometer closest to the channel. P.O.:'--' designates a negligible oscillatory response (< 5 mm amplitude).

As the aim is to study specifically the oscillatory responses to the tidal signal, one can extract these oscillatory responses from the measurements by subtracting the linear responses, obtained through a linear regression. Then, one can assess the amplitude and phase-offset values of the isolated oscillatory responses by performing a fast Fourier transform (FFT) on them, as the period of the sea tidal signal (12.2 hours) at this location is known from the French Naval Hydrographic and Oceanographic Service data. Examples of the data processing undertaken on four different piezometer measurements are presented in Figure 3.

Once the amplitude and phase-offset responses to the tidal signal for each piezometer have been extracted, it is possible to create a map of spatial intensity of these responses (Figure 4).

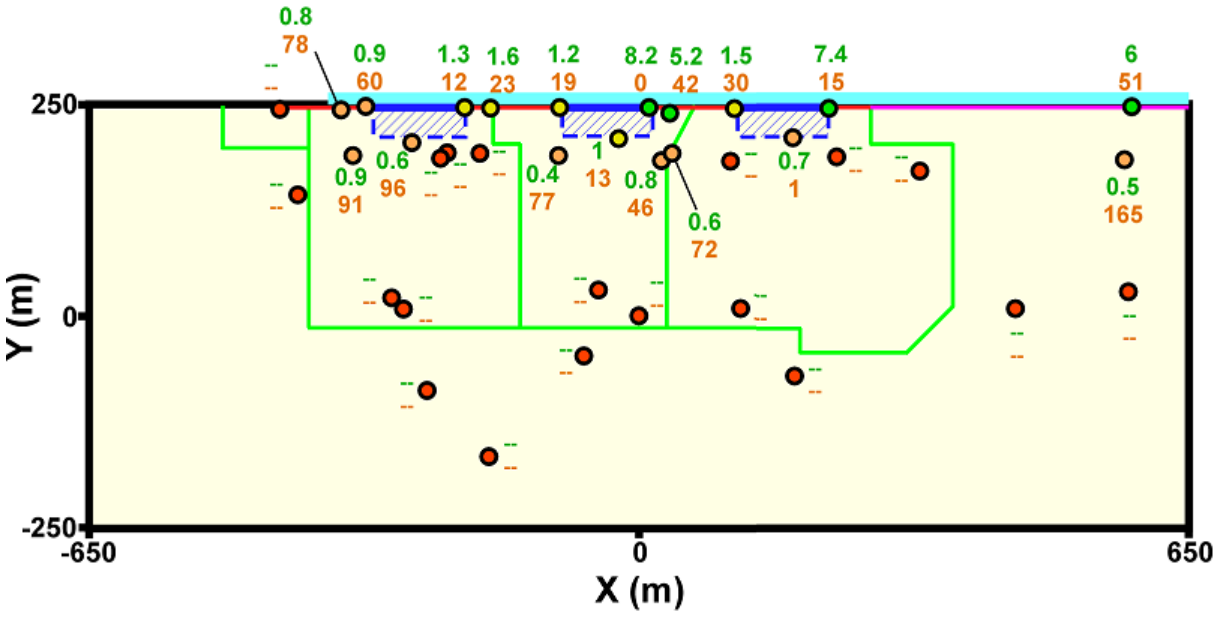

Figure 4: Amplitude and phase-offset responses interpreted from the signals of each piezometer on the site. The amplitude responses in green are in cm, the phase-offset responses in orange are in degrees (°). Green circles designate responses with amplitudes higher than 2 cm, yellow circles designate amplitudes between 1 and 2 cm, and orange circles designate amplitudes between 0.5 and 1 cm. The red circles with '--' designate responses with a negligible amplitude (< 5 mm).

From this map, it appears that piezometers closer to the channel show more intensive oscillatory responses. This shows that the oscillatory responses measured from the piezometers are indeed responses to the tidal signal of the channel. In contrast, piezometers that are located more than 125 m away from the channel do not respond to its signal, which has attenuated in the aquifer. This means that the tidal signal will only permit characterization of a band of approximately 125 m alongside the channel.

The intensities and the phase lags of the responses directly along the channel are very variable. This effect can be attributed to the hydraulic barriers along the channel, and more specifically to a spatial variation of the efficiency of these barriers.

It also appears from this map that the amplitude response decreasing when moving away from the channel is generally associated to an increasing phase-offset response. This observation is in agreement with several other works on oscillatory responses (Renner and Messar 2006 ; Rabinovich et al. 2015 ; Zhou et al. 2016 ; Fischer et al. 2018a). Two boreholes, P19 and P23, present a low amplitude associated to a low phase offset. This could be attributed to a cycle delay in the phase. This hypothesis can be verified in the following modeling simulations.

The next step of this study aims to interpret the distribution of amplitude and phase-offset responses over the field in terms of distribution of transmissivity and storativity. This can be performed with an inversion process in a numerical model.

3. Modeling strategy

3.1. Forward problem and model parameterization

This study aims to reproduce the measured amplitude and phase-offsets in the oscillatory responses in a 2D model, in order to map the distribution of the transmissivity and storativity properties of the aquifer and the anthropic structures in the field.

In order to reduce the computation time when solving the model, the numerical modeling is performed in a frequency domain. In fact, the oscillatory responses can be rewritten in complex form as follows:

$$h_{\text{osc.}}(x,y,t)=A(x,y)\cos\left(\omega t-\Phi(x,y)\frac{\pi}{180}\right)=\text{Re}\left(H_{\omega}(x,y)\,e^{i\omega t}\right) \quad (2)$$

with A the amplitude of the signal in m, Φ the phase offset of the signal in °, ω the angular frequency of the signal in rad.s^{-1}, H_{ω} the complex variable carrying the oscillatory responses in the frequency domain, Re the real part of a complex number and i the imaginary unit.

The 2D model is built with the software COMSOL Multiphysics. The dimensions of the model are presented in Figure 2, with the channel considered as a linear boundary condition. This model is enclosed in a buffer zone of dimensions 3000×2000 m² and associated with uniform regional aquifer properties, which permits limitation of the impact of the other external boundary conditions. The aquifer properties are represented in 2D in the model, while the anthropic structures' properties are represented in 1D along lines representing the walls and barriers presented in Figure 1.

The groundwater flows are simulated using the continuity equation in the frequency form, considering Darcy's law and the following initial and boundary conditions:

$$\begin{cases} i\omega S(x,y)H_\omega(x,y)-\nabla\left(T(x,y)\nabla H_\omega(x,y)\right)=0 & \text{in 2D} \\ i\omega S_{\text{barrier}}(x,y)H_\omega(x,y)-\nabla\left(T_{\text{barrier}}(x,y)\nabla H_\omega(x,y)\right)=0 & \text{in 1D} \end{cases} \quad (3)$$

$$\text{with } H_{\omega,\text{init.}}(x,y)=0 \quad \text{and} \begin{cases} H_\omega(x,y)_{\text{channel}}=0.082 \\ H_\omega(x,y)_{\text{bound.}}=0 \end{cases}$$

with S the storativity (no unit), T the transmissivity in $m^2.s^{-1}$, S_{barrier} and T_{barrier} being related to the 1D barrier structures in the model. $H_{\omega,\text{init.}}$, $H_\omega(x,y)_{\text{channel}}$, $H_\omega(x,y)_{\text{bound.}}$ are the initial and boundary conditions of the model. The value for the channel condition is chosen according to the oscillation generated by the channel in the soil. As the barriers might have produced local non-Darcian effects on the flows, and as Darcy flows are considered in the simulations, it is more correct to refer to S_{barrier} and T_{barrier} as equivalent storativities and transmissivities incorporating these non-Darcian effects. However, as the aim is to characterize these structures and their relative efficiency in space rather than their exact values, equivalent properties are sufficient.

The resolution of the model is performed with a finite element method, along a triangular mesh.

The amplitude and phase-offset spatial simulations can then be extracted following the formulas:

$$\begin{cases} A(x,y)=\sqrt{\left(\text{Re}H_\omega(x,y)\right)^2+\left(\text{Im}H_\omega(x,y)\right)^2} \\ \Phi(x,y)=\dfrac{180}{\pi}\text{atan2}\left(-\text{Im}H_\omega(x,y),\text{Re}H_\omega(x,y)\right) \end{cases} . \quad (4)$$

Im represents the imaginary part of a complex number and atan2 is the 2-argument arctangent function. The spatial oscillatory responses in the time domain can be reconstructed using the amplitudes and phase-offsets simulated in the frequency domain and the formula in Eq. 2.

3.2. Inverse problem

The distributions of the transmissivity and storativity properties in the model are reconstructed through an inversion process. Therefore the property values distributed over a regular grid composed of rectangular cells (aquifer) and over lines composed of regular segments (structures) are stored in a vector $\mathbf{p}$. The deterministic optimization that consists of modifying the values in $\mathbf{p}$ in order to improve the reproduction of the measured responses with the model, is then performed through an iterative process that aims at minimizing the following objective function:

$$\Psi = \left(\mathbf{d}_{\text{obs.}} - f\left(\mathbf{p}\right)\right)^{\mathrm{T}} \mathbf{C}_{\mathrm{d}}^{-1} \left(\mathbf{d}_{\text{obs.}} - f\left(\mathbf{p}\right)\right) + \left(\mathbf{p}_{\text{prior}} - \mathbf{p}\right)^{\mathrm{T}} \mathbf{C}_{\mathrm{p}}^{-1} \left(\mathbf{p}_{\text{prior}} - \mathbf{p}\right) \tag{5}$$

with $\mathbf{d}_{\text{obs.}}$ and $f\left(\mathbf{p}\right)$ the n-vectors containing respectively the measured and simulated amplitude and phase offset responses, $\mathbf{p}$ and $\mathbf{p}_{\text{prior}}$ the m-vectors containing respectively the S and T distributions in the model and their *a priori* distributions, and $\mathbf{C}_{\mathrm{d}}$ and $\mathbf{C}_{\mathrm{p}}$ the $n \times n$ and $m \times m$ matrices of covariance on the set of responses and the property distribution, respectively.

As the deterministic inversion is iterative, it is first necessary to initialize the values in $\mathbf{p}$ with reasonable property values. Then, at a given iteration step k, the property values in $\mathbf{p}$ can be optimized considering the values from the previous step with a linearization using a first-order Taylor approximation:

$$\begin{aligned} & f\left(\mathbf{p}_{k+1}\right) \simeq f\left(\mathbf{p}_{k}\right) + \mathbf{F}_{k}\left(\mathbf{p}_{k+1} - \mathbf{p}_{k}\right) \\ & \text{where} \quad \mathbf{F}_{k}\left(i,j\right) = \left.\frac{\partial f_{i}}{\partial \mathbf{p}_{k}}\right|_{\mathbf{p}_{k}(j) = \mathbf{p}_{k}(j) + \Delta p} \end{aligned} \tag{6}$$

with $\mathbf{p}_k$ and $\mathbf{p}_{k+1}$ the property distribution at iterations k and $k+1$, $\mathbf{F}_k$ the $n \times m$ Jacobian matrix calculated at iteration k with a finite-difference method, and Δp the finite difference step.

Then, $\mathbf{p}_{k+1}$ is calculated as:

$$\mathbf{p}_{k+1} = \mathbf{p}_k + \left(\mathbf{F}_k{}^{\mathrm{T}}\mathbf{C}_{\mathrm{d}}{}^{-1}\mathbf{F}_k + \mathbf{C}_{\mathrm{p}}{}^{-1}\right)^{-1}.\left(\mathbf{F}_k{}^{\mathrm{T}}\mathbf{C}_{\mathrm{d}}{}^{-1}\left(\mathbf{d}_{\mathrm{obs.}} - f\left(\mathbf{p}_k\right)\right) + \mathbf{C}_{\mathrm{p}}{}^{-1}\left(\mathbf{p}_{\mathrm{prior}} - \mathbf{p}_k\right)\right) \quad (7)$$

Finally, once the objective function has been sufficiently minimized, the optimization iterations are stopped. The uncertainties on the final property values in $\mathbf{p}$ can be estimated as follows:

$$\mathbf{p}_{\mathrm{uncert.}}(i) = \sqrt{\mathbf{C}_{\mathrm{p,post}}(i,i)} \quad \text{where} \quad \mathbf{C}_{\mathrm{p,post}} = \left(\mathbf{F}_{\mathrm{post}}{}^{\mathrm{T}}\mathbf{C}_{\mathrm{d}}{}^{-1}\mathbf{F}_{\mathrm{post}} + \mathbf{C}_{\mathrm{p}}{}^{-1}\right)^{-1} \quad (8)$$

with $\mathbf{p}_{\mathrm{uncert.}}$ the m-vector of standard deviations associated to the property values of the final model, $\mathbf{C}_{\mathrm{p,post}}$ the $m \times m$ matrix of posterior covariance on the property distribution, and $\mathbf{F}_{\mathrm{post}}$ the Jacobian matrix calculated during the last iteration.

3.3. Inversion parameters

The inversion algorithm is coded with MATLAB and performed using the MATLAB/COMSOL connection to solve the forward model. The different values of inversion parameters chosen for this study case are presented in Table 1.

The property values to be optimized in the model are distributed, for the aquifer, over a grid composed of 2000 rectangular cells, and for the walls located along the channel, over a line composed of 100 regular segments. All other buried structures existing as 1D lines in the model are considered as a unique entity in the inversion, thus associated to uniform values of equivalent properties. In this way, 4200 unknown transmissivities and storativities will be

282 considered in the inversion process. This resolution allows for sufficient liberty, in order to
283 reproduce the complexity of the field flows, while also keeping an acceptable duration of the
284 inversion process.

285 Table 1: Parameter values used for the inverse modeling.

Parameter	Value
Data uncertainty	$\pm$ 0.1 cm on amplitude $\pm$ 10° on phase-offset
Property distribution resolution	100 $\times$ 20 cells distributed over $X \in$ [-450 ; 650] and $Y \in$ [125 ; 250]
Property distribution variogram function	$\mathrm{Var}(\mathrm{distance}) = 0.1 \times \left[1 - \exp\left(-\frac{\mathrm{distance}}{8}\right)\right]$
Buried walls (channel) property resolution	100 segments
Buried structures' property variance	$\boldsymbol{\sigma}^2_{\mathrm{str}} = 10^{-1}$
Initial transmissivities	Aquifer: 3.10^{-6} m²/s; Structure: 10^{-9} m²/s ; Building: 10^{-7} m²/s
Initial storativities	Aquifer: 5.10^{-5}; Structure: 10^{-2} ; Building: 10^{-3}
Finite difference step	10^{-5}
Buffer zone	$T = 3.10^{-6}$ m²/s ; $S = 5.10^{-5}$

286

287 The vectors $\mathbf{p}$ and $\mathbf{p}_{\mathrm{prior}}$ are built using the $-\log_{10}$ values of transmissivity and storativity
288 presented in Table 1. The initial property values are also used as a priori values for the inversion
289 in $\mathbf{p}_{\mathrm{prior}}$. These initial values are chosen according to values presented for regional studies of
290 this aquifer, while the structure and building equivalent properties are set voluntarily to low T
291 and high S in order to lower flows through these parts of the model.

292 The covariance matrix $\mathbf{C}_{\mathrm{d}}$ is built as a diagonal matrix. Its diagonal entries are the data
293 uncertainty values (Table 1) associated, respectively, to the amplitude responses and the phase-
294 offset responses in $\mathbf{d}$ and $\mathbf{d}_{\mathrm{obs.}}$. The covariance matrix $\mathbf{C}_{\mathrm{p}}$ is built as a variogram matrix for

its parts associated to the aquifer properties and as a diagonal matrix for the parts associated to the structures' properties. Its variogram part is calculated with the variogram function (Table 1), by taking into account the distances between each cell of the property grid. This variogram remains voluntarily permissive, in order to allow for some spatial variations while also avoiding discontinuities in the distribution. Its diagonal part is built with the buried structures' property variance value (Table 1).

Two inversions were performed: one taking into account the three buildings along the channel by considering specific ('building') initial property values in their zones, and one not taking them into account by considering the 'aquifer' initial properties in their zones. An impact of the building structures on the groundwater flows is in fact not certain, therefore it is interesting to perform these two inversions.

4. Results and discussion

4.1. Comparing models with or without integrating buildings

The transmissivity and storativity maps derived from the inversion processes are presented respectively in Figure 5 and Figure 6. The reproduction of the 37 measured responses with these models is presented in Figure 7.

Note that the distributions of the properties in the aquifer are very heterogeneous and in a wide range of values (from 10^{-4} m²/s to 10^{-6} m²/s for the transmissivities and from 10^{-3} to 10^{-6} for the storativities).

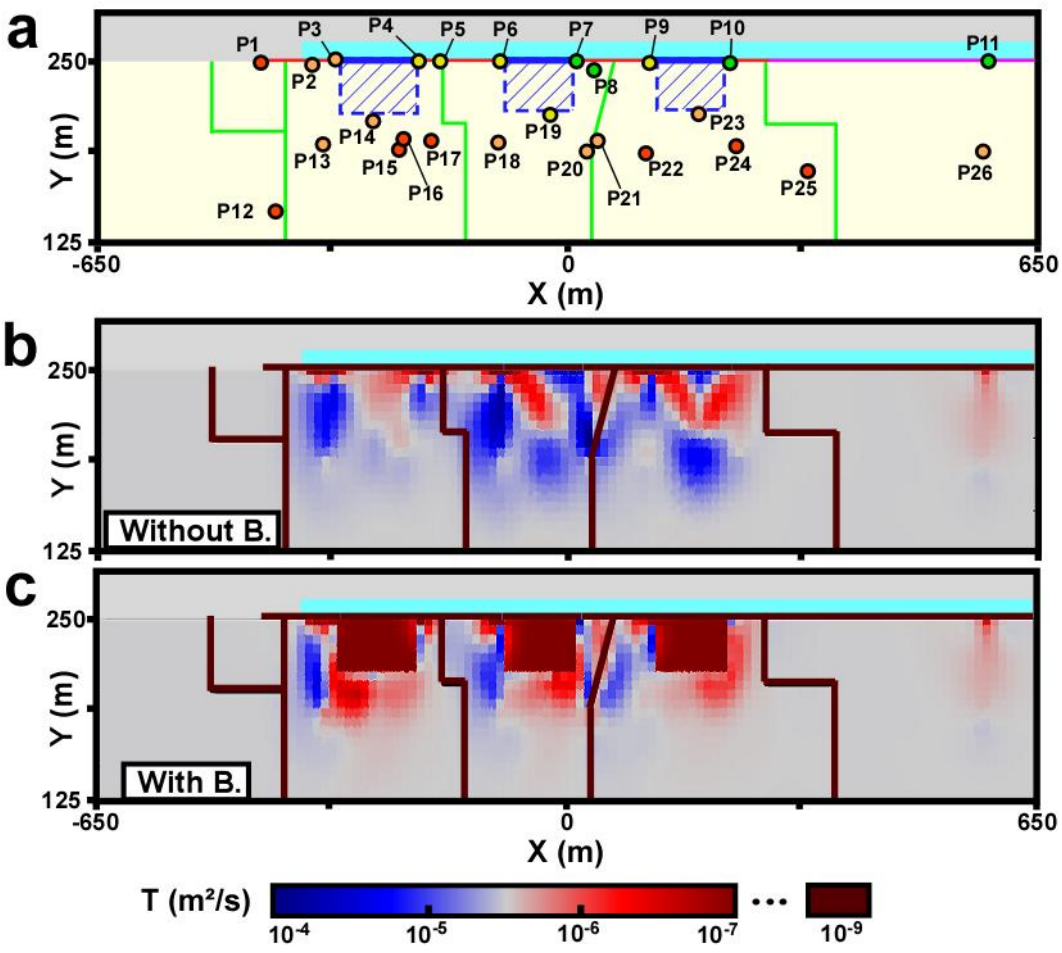

315

316 Figure 5: **a** The location of the piezometers in the (zoomed-in) zone near the channel. Maps of
317 inverted transmissivities (*T*) for the inversions **b** taking into account the buildings (With B.)
318 and **c** not taking into account the buildings (Without B.).

319

320 In the inversion 'without buildings' it is observed that a low transmissivity has been attributed
321 to the area of the buildings and that the two transmissivity maps (with and without buildings)
322 present different distributions in the areas surrounding the buildings (especially on their side
323 opposite the channel). Therefore, concerning the transmissivity distribution, taking into account
324 the buildings as *a priori* knowledge, does significantly modify the result of the inversion.

325 Concerning the storativity distribution, it is noted that neither the 'without building' distribution
326 increases the storativity values in the building areas, nor the areas surrounding the buildings is
327 different between the results of the inversions 'with buildings' or 'without buildings'. Then,

328 contrarily to the transmissivity distribution, taking into account the buildings as *a priori*
329 knowledge does not seem to impact significantly the inversion of the storativity distribution.
330 This suggests that the flows in the aquifer in the buildings area are mostly driven by the
331 transmissivity.

332 It is also interesting to observe that the distribution of the blue zones (high transmissivity, low
333 storativity) and the red zones (low transmissivity, high storativity) in Figures 5 and 6 is much
334 more coherent in the results of the inversion 'with buildings'. The distributions of the blue and
335 red zones in the transmissivity and storativity maps inverted in this case are, indeed, much more
336 similar than in the results of the inversion 'without buildings'.

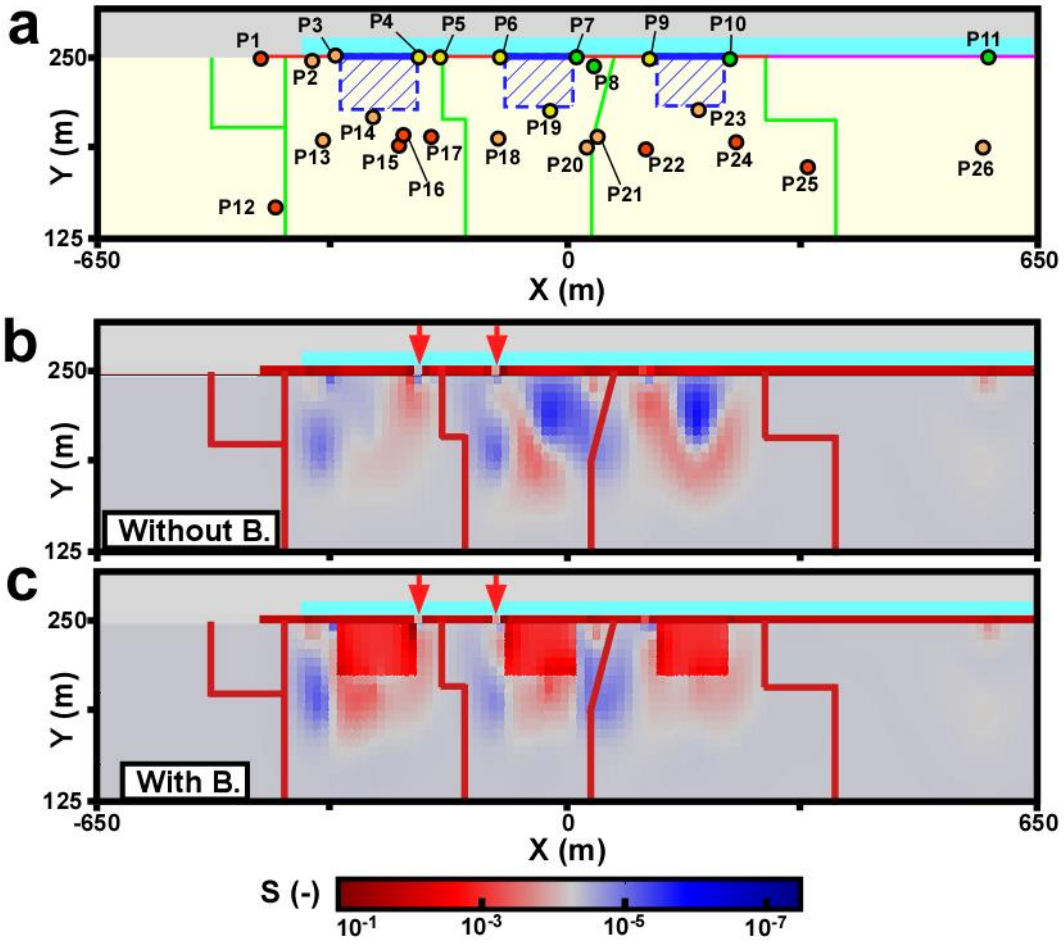

Figure 6: **a** The location of the piezometers in the (zoomed-in) zone near the channel. Maps of inverted storativities (*S*) for the inversions **b** taking into account the buildings (With B.) and **c** not taking into account the buildings (Without B.). The red arrows designate the less efficient segments of the anthropic structures in the model.

Concerning the distribution of the equivalent properties along the different anthropic structures, the optimization process modified the storativity values more than the transmissivity values. In fact, the equivalent storativity values in the results range from 10^{-1} to 10^{-4}, while the equivalent transmissivity values remain close to the initial value 10^{-9} m²/s. The distribution of the equivalent storativities along the walls in the model is therefore more relevant to localization of the more and less efficient parts of the hydraulic barrier constructed along the channel. The red arrows in Figure 6 show the localization of the relatively less efficient parts of the barriers

in the two inversion results. It was first observed that these localizations are exactly the same in both results, which indicates again that the buildings' a priori information do not significantly affect the inversion of the storativity distribution. The two relatively less efficient parts of the hydraulic barriers are located at the junctions between buttress walls and cutoff walls, thus they could be associated to the sealing between these walls.

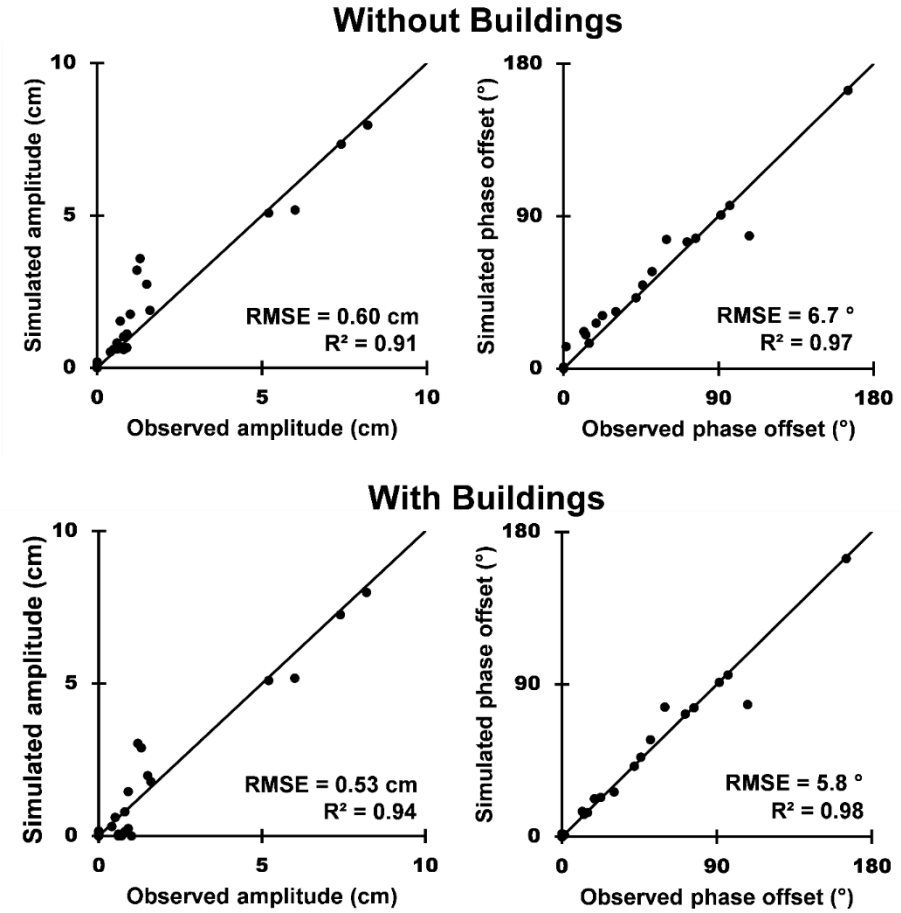

Figure 7: Amplitudes and phase-offsets measured versus amplitudes and phase-offsets simulated with the property distributions presented in Figures 5 and 6. Each graph is associated to the values of R^2 and root mean square error (RMSE) between the simulated and measured data.

Globally the reproduction of the amplitude and phase offset responses is very similar with the property maps inverted with or without the buildings. However, the model 'with buildings',

365 incorporating an *a priori* knowledge, provides a slightly better simulation of the measured
366 responses.

367 The transmissivity distributions in these results (Figure 5) and the responses' reproduction
368 (Figure 7) suggest that the local decrease of transmissivity induced by the buildings is necessary
369 in the model to simulate its impact on the groundwater flows. Therefore, the rest of the article
370 addresses essentially the model of the inversion 'with buildings', which seems to provide more
371 reliable results in this case.

372 ## 4.2. Exploring the impact of buildings on the tidal signal propagation

373 Figure 8 presents the simulations of amplitude and phase-offset responses obtained with the
374 property maps of the model 'with buildings'.

375 The simulations run with the model are able to represent the complexity and the heterogeneity
376 of the site. The amplitude of the tidal signal 'enters' the aquifer only through the buttress walls,
377 between the buildings, thereby the amplitude response to this signal dissipates to an
378 undetectable level very close to the channel in the building zones. Furthermore, the propagation
379 of the signal in the aquifer along the buttress walls is also very different alongside the channel;
380 it depends on the distribution of the properties of the aquifer in the model. The propagation of
381 the tidal signal in the aquifer is then a combination of the efficiency of the hydraulic barriers
382 and of the distribution of the property behind the barrier. In fact, it can be observed that the
383 relatively less efficient parts of the hydraulic barriers highlighted in Figure 6 do not necessarily
384 match with the areas where the tide signal can be the most observed in the aquifer. Therefore it
385 is interesting to invert these entities simultaneously.

386 The phase-offset simulations permit better visualization of the propagation of the tidal signal.
387 It shows that the signal enter through the buttress walls, then continues between the buildings
388 and the impermeable screens orthogonal to the channel, and finally encircles the back of the

389 buildings and continues propagating behind. The phase-offsets simulated behind the buildings
390 can be delayed by an entire period compared to the channel signal according to these
391 simulations. This propagation behavior could explain why, even if the buildings completely
392 stop the tidal signal, one can still measure responses with a small phase-offset in piezometers
393 just behind these ones: they correspond to responses with a full cycle of delay (see P19 and
394 P23).

395

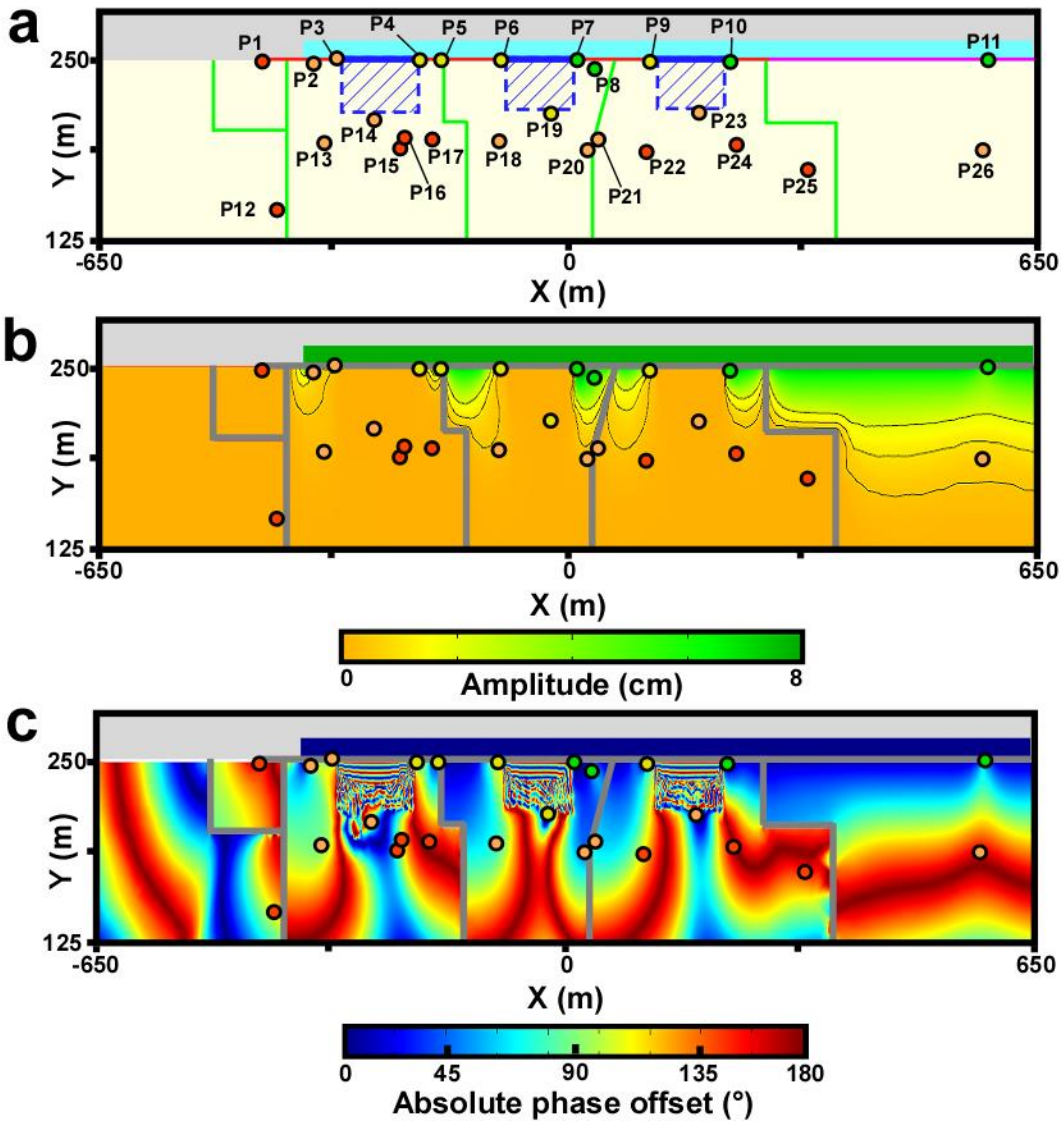

396

397 Figure 8: **a** The location of the piezometers in the (zoomed-in) zone near the channel. Maps of
398 the simulated **b** amplitude and **c** phase-offset responses with the property distributions 'with
399 buildings' presented in Figures 5 and 6.

The maps of simulations also explain the differences of responses on each side of the impermeable screens orthogonal to the channel. These barriers have a non-negligible impact on the propagation of the signal in the aquifer, as can be clearly observed on the amplitude response simulation. Therefore, integrating the barriers as 1D elements in the model and the inversion process are very useful to explain some particular flow interactions between the aquifer and the anthropic structures (like the phase lag between the two very close piezometers P20 and P21).

4.3. Quantifying uncertainties in the model around the channel and buildings

One crucial part of characterization is the study of the posterior covariance on the properties of the model, which provides the spatial uncertainties on the property values. Therefore, study of posterior covariance provides an indication of the spatial accuracy of the distributions found through the inversion process. Figure 9 shows the maps of standard deviations on the values of transmissivity and storativity calculated for the inversion ‘with buildings’.

First of all, one observes that the inverted distribution of properties is more accurate alongside the channel, which is logical because the measured responses in the aquifer are more important in this area. The building locations are associated with high uncertainty, which appears logical as they were voluntarily initially associated with very low transmissivities and high storativities. Thus, a slight modification of their property value will not generate a significant change on the flows. In the aquifer part, the transmissivities are better constrained than the storativities, while in the anthropic barriers parts the storativities are better constrained than the transmissivities. In both parts, the areas that are most constrained are located in the surroundings of the buildings and at the positions of the responding piezometers.

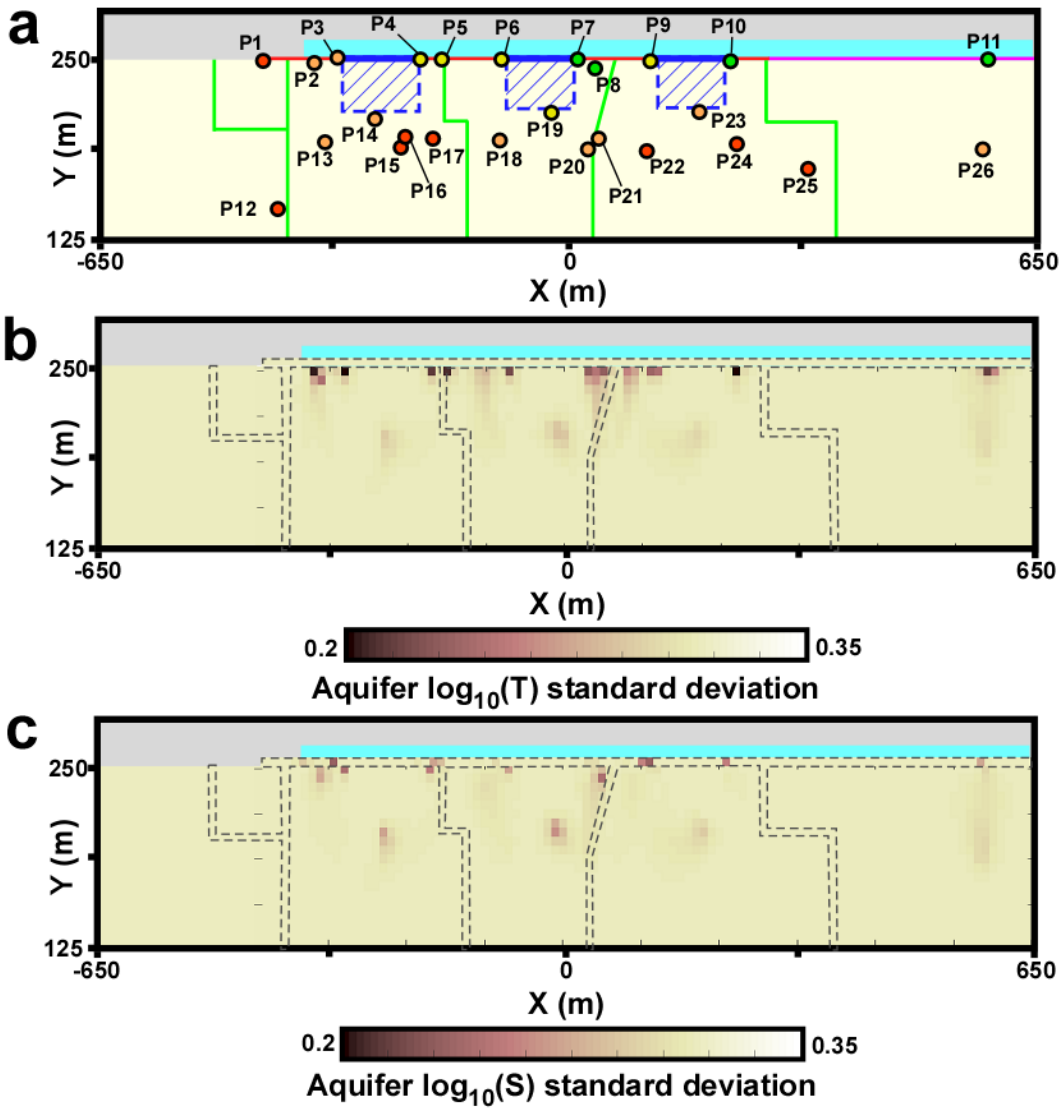

Figure 9: **a** The location of the piezometers in the (zoomed-in) zone near the channel. Maps of the **b** transmissivity (*T*) and **c** storativity (*S*) standard deviations on the property distributions 'with buildings' presented in Figures 5 and 6.

The inverted model seems to be reliable in the areas around the buildings, in the center part of the model, between the anthropic structures. In fact, in these areas, the flows appear to be constrained and there is a sufficient number of piezometers to characterize these flows. However the areas on the left and on the right of the model seem to be rather unreliable. In these two zones, there are only two piezometers to measure the aquifer responses and, if the properties

found in the direct vicinity of these two piezometers are well constraint, most of these areas cannot be well characterize because of a lack of information. In order to reduce the uncertainties of the model near the channel, more piezometer measuring responses in the aquifer would be necessary.

Finally, the parts of the site located far (> 100 m away) from the channel, in which no oscillatory responses to the tidal signal could be measured in the piezometers, are not well constraint in the model, and therefore inaccurate. Thus, as already suggested in section '*Data processing'*, the tidal signal from the channel does not permit characterization of areas very far away from it. Cardiff and Barrash (2015) proposed analytical tools in order to design punctual oscillatory sources for aquifer characterizations. At the site used in this study, the oscillatory source is not punctual and the aquifer heterogeneous, however these tools can give an idea of the distance investigable with the channel source. According to the period of tidal signal and the mean property values of the aquifer, the distance of signal propagation should be around 75 m, which seems coherent to what was observed. In order to better characterize the aquifer far from the channel, other sources of signals (such as active pumping or slug tests) would be required.

4.4. Discussion

Some prerequisites and precautions should be considered when choosing to apply this characterization strategy. As shown in this paper, only a limited area alongside the channel can be characterized using tidal signals; more-inland zones require other sources of signal. Furthermore, in order to produce a reliable map of the property distributions, this method requires a larger number of measurement piezometers, spatially well-distributed along the channel. Finally, the incorporation of *a priori* knowledge regarding property distribution appears to be useful to generate more coherent and realistic models, as shown in this work with the integration of the building foundations as *a priori* information in the inversion process.

The presented characterization method, based only on the channel as a solicitation signal at the boundary of the model, permits characterization of the spatial distribution of the aquifer properties without having to perform an active solicitation techniques (pumping, slug tests, etc.), which is especially interesting in cases where the use of such techniques is limited or impossible. The hydraulic characterization presented in this study also presents the advantage of simultaneously characterizing the properties of the aquifer (in 2D) and of the anthropic structures and barriers (in 1D) alongside the channel. This can enhance the success of the inversion process and localize the relatively less efficient segments of the barriers.

5. Conclusion

The tidal signal carried by the channel connected to the sea has been exploited in this study to characterize a highly anthropized coastal field, without any active solicitation (such as pumping tests). Data processing on the piezometric measurements in the aquifer enabled extraction of the groundwater responses, specifically to this tidal signal, in terms of amplitude and phase-offset values. The numerical model, solved in a frequency domain and associated to property distributions generated by inversion of the responses to the tidal signal, could finally allow for an interpretation of the propagation of the signal through the anthropic barriers and in the aquifer. The integration of the anthropic structures as 1D elements in the model and of *a priori* information of the buildings foundations in the inversion process generate a more realistic model, able to simulate the complex behavior of the propagation of the tidal signal between the buildings and barriers within the aquifer. The maps of simulated propagation of signal, generated from the inverted model of properties, represent, in the end, an interesting tool in order to understand and interpret the responses measured punctually in the field. These maps can help to understand how the groundwater flows under the site, near the channel, which allows for better water resource management.

Acknowledgments

We thank EDF for their financial support for this work. Data presented in this article are property of EDF. The code is accessible upon request to the corresponding author.

References

Alcolea A., E. Castro, M. Barbieri, J. Carrera, S. Bea. 2007. Inverse Modeling of Coastal Aquifers Using Tidal Response and Hydraulic Tests. *Ground Water* 45: 711-722.

Black J.H., K.L. Kipp. 1981. Determination of hydrogeological parameters using sinusoidal pressure tests: A theoretical appraisal. *Water Resources Research* 17: 686-692.

Black J.H., D.C. Holmes, M.A. Brightman. 1987. Crosshole investigations: Hydrogeological results and interpretations (STRIPA-TR--87-18). Sweden

Bolève A., F. Janod, A. Revil, A. Lafon, J.-J. Fry. 2011. Localization and quantification of leakages in dams using time-lapse self-potential measurements associated with salt tracer injection. *Journal of Hydrology* 403: 242-252.

Bouwer H., and R. C. Rice. 1976. A Slug Test for Determining Hydraulic Conductivity of Unconfined Aquifers With Completely or Partially Penetrating Well. *Water Resource Research* 12: 423-428.

Brauchler R., R. Hu, T. Vogt, D. Al-Halbouni, T. Heinrichs, T. Ptak, M. Sauter. 2010. Cross-well slug interference tests: An effective characterization method for resolving aquifer heterogeneity. *Journal of Hydrology* 384: 33-45.

508 Cardiff M., W. Barrash, P. K. Kitanidis, B. Malama, A. Revil, S. Straface, E. Rizzo. 2009. A
509 Potential-Based Inversion of Unconfined Steady-State Hydraulic Tomography. *Ground Water*
510 47: 259-270.

511

512 Cardiff M., T. Bakhos, P. K. Kitanidis, W. Barrash. 2013. Aquifer heterogeneity
513 characterization with oscillatory pumping: sensitivity analysis and imaging potential. *Water*
514 *Resources Research* 49: 5395-5410.

515

516 Cardiff, M., W. Barrash. 2015. Analytical and Semi-Analytical Tools for the Design of
517 Oscillatory Pumping Tests. *Groundwater* 53: 896-907.

518

519 Carrera J., and S. P. Neuman. 1986. Estimation of aquifer parameters under transient and steady
520 state conditions: 3.Application to synthetic and field data. *Water Resources Research* 22: 228-
521 242.

522

523 De Marsily, G., A. M. LaVenue, B. S. RamaRao, M. G. Marietta. 1995. Pilot point methodology
524 for automated calibration of an ensemble of conditionally simulated transmissivity fields:
525 2.Application. *Water Resources Research* 31: 495-516.

526

527 D'Oria M., A. Zanini. 2019. Characterization of hydraulic heterogeneity of alluvial aquifer
528 using natural stimuli: A field experience of Northern Italy. *Water* 11: 176.

529

530 Fischer P., A. Jardani, A. Soueid Ahmed, M. Abbas, X. Wang, H. Jourde, N. Lecoq. 2017.
531 Application of Large-Scale Inversion Algorithms to Hydraulic Tomography in an Alluvial
532 Aquifer. *Groundwater* 55: 208-218.

533

534 Fischer P., A. Jardani, M. Cardiff, N. Lecoq, H. Jourde. 2018a. Hydraulic analysis of harmonic
535 pumping tests in frequency and time domains for identifying the conduits networks in a karstic
536 aquifer. *Journal of Hydrology* 559: 1039-1053.

537

538 Fischer P., A. Jardani, H. Jourde, M. Cardiff, X. Wang, S. Chedeville, N. Lecoq. 2018b.
539 Harmonic pumping tomography applied to image the hydraulic properties and interpret the
540 connectivity of a karstic and fractured aquifer (Lez aquifer, France). *Advances in Water*
541 *Resources* 119: 227-244.

542

543 Guiltinan E., and M. W. Becker. 2015. Measuring well hydraulic connectivity in fractured
544 bedrock using periodic slug tests. *Journal of Hydrology* 521: 100-107.

545

546 Illman W. A., X. Liu, S. Takeuchi, T.-C. J. Yeh, K. Ando, H. Saegusa. 2009. Hydraulic
547 tomography in fractured granite: Mizunami Underground Research site, Japan. *Water*
548 *Resources Research* 45: W01406. doi: 10.1029/2007WR006715.

549

Jardani A., J. P. Dupont, A. Revil, N. Massei, M. Fournier, B. Laignel. 2012. Geostatistical inverse modeling of the transmissivity field of a heterogeneous alluvial aquifer under tidal influence. *Journal of Hydrology* 472-473: 287-300.

Rabinovich A., W. Barrash, M. Cardiff, D. L. Hochstetler, T. Bakhos, G. Dagan, P. K. Kitanidis. 2015. Frequency dependent hydraulic properties estimated from oscillatory pumping tests in an unconfined aquifer. *Journal of Hydrology* 531: 2-16.

Renner J., and M. Messar. 2006. Periodic pumping tests. *Geophysical Journal International* 167: 479-493.

Rhoads Jr. G. H., and E. S. Robinson. 1979. Determination of aquifer parameters from well tides. *Journal of Geophysical Research* 84: 6071-6082.

Sun A. Y., J. Lu, S. Hovorka. 2015. A harmonic pulse testing method for leakage detection in deep subsurface storage formations. *Water Resources Research* 53: 4263-4281.

Tarantola A., and B. Valette. 1982. Generalized nonlinear inverse problems solved using the least squares criterion. Reviews of Geophysics and Space Physics 20: 219-232.

Tefry M. G., and E. Bekele. 2004. Structural characterization of an island aquifer via tidal methods. Water Resources Research 40: W01505. doi:10.1029/2003WR002003.

572

573 Vilarrasa V., J. Carrera, A. Jurado, E. Pujades, E. Vázquez-Suné. 2011. A methodology for
574 characterizing the hydraulic effectiveness of an annular low-permeability barrier. *Engineering*
575 *Geology* 120: 68-80.

576

577 Wang C.-Y., M.-L. Doan, L. Xue, A. J. Barbour. 2018. Tidal Response of Groundwater in a
578 Leaky Aquifer – Application to Oklahoma. *Water Resources Research*.
579 doi:10.1029/2018WR022793.

580

581 Wen J.-C., H.-R. Lin, T.-C. J. Yeh, Y.-L. Wang, K.-L. Lin, S.-Y. Huang. 2018. Hydraulic
582 Tomography for Estimating the Diffusivity of Heterogeneous Aquifers Based on Groundwater
583 Response to Tidal Fluctuation in an Artificial Island in Taiwan. *Geofluids* 2018:
584 doi:10.1155/2018/6046258.

585

586 Yeh T.-C. J., and C.-H. Lee. 2007. Time to Change the Way We Collect and Analyze Data for
587 Aquifer Characterization. *Ground Water* 45: 116-118.

588

589 Zhou, Y., D. Lim, F. Cupola, M. Cardiff. 2016. Aquifer imaging with pressure waves-
590 Evaluation of low-impact characterization through sandbox experiments. *Water Resources*
591 *Research* 52: 2141-2156.

592